UNIVERSIDAD NACIONAL DE COLOMBIA

Automatic 3D segmentation of the prostate on magnetic resonance images for radiotherapy planning

Charlens Alvarez Jiménez

Universidad Nacional de Colombia
Facultad de Medicina, Departamento de Imagenes Diagnosticas
Bogota, Colombia
2014

Automatic 3D segmentation of the prostate on magnetic resonance images for radiotherapy planning

Charlens Alvarez Jiménez

In fulfillment of the requirements for the degree of:
Magister en Ingeniería Biomédica

Advisor:
Ph.D. MD. Eduardo Romero Castro

Research Field:
Applied Computing - Image Processing
Research Group:
Computer Imaging and Medical Applications Laboratory - CIM@LAB

Universidad Nacional de Colombia
Facultad de Medicina, Departamento de Imagenes Diagnosticas
Bogota, Colombia
2014

A mis padres Luz Marina y Pablo
A mis hermanitas Joha y Jessy
A mi esposo Jonathan
Y a mis abuelitas,
presentes siempre en mi corazón

Acknowledgments

First, I want to express my sincerest gratitude to my advisor Eduardo Romero, who allowed me to make my dreams come true. Thanks for his continuous support, motivation, thoughtful guidance and for his patience when I felt falter. Besides my advisor, I would like to thank Fabio Martinez for the trust, the insightful discussion, offering valuable advice, for his support during the whole period of the study, and especially for his patience during the writing process.

I also thank people from the CIM@LAB laboratory: Andrea Rueda, Josue Ruano, Nelson Velazco, Jorge Alvarez, Luisa Cardenas, David Trujillo, Andrea Pulido, Juan David and Katherine Baquero for their insightful comments, critical suggestions, hard questions and for their invaluable support during this process.

I take this opportunity to express the profound gratitude to my husband Jonathan Tarquino for his encouragement, excellent advice and detailed review during the preparation of this thesis, and to my family and friends Lucia, Angie, David, Jeffrey, Bladimir, John y Andrea Hurtado for supporting me throughout all my studies.

Abstract

Accurate segmentation of the prostate, the seminal vesicles, the bladder and the rectum is a crucial step for planning radiotherapy (RT) procedures. Modern radiotherapy protocols have included the delineation of the pelvic organs in magnetic resonance images (MRI), as the guide to the therapeutic beam irradiation over the target organ. However, this task is highly inter and intra-expert variable and may take about 20 minutes per patient, even for trained experts, constituting an important burden in most radiological services. Automatic or semi-automatic segmentation strategies might then improve the efficiency by decreasing the measured times while conserving the required accuracy. This thesis presents a fully automatic prostate segmentation framework that selects the most similar prostates w.r.t. a test prostate image and combines them to estimate the segmentation for the test prostate. A robust multi-scale analysis establishes the set of most similar prostates from a database, independently of the acquisition protocol. Those prostates are then non-rigidly registered towards the test image and fusioned by a linear combination. The proposed approach was evaluated using a MRI public dataset of patients with benign hyperplasia or cancer, following different acquisition protocols, namely 26 endorectal and 24 external. Evaluating under a leave-one-out scheme, results show reliable segmentations, obtaining an average dice coefficient of 79%, when comparing with the expert manual segmentation.

Keywords: Radiotherapy planning, MRI prostate segmentation, atlas based approaches, label fusion strategy.

Resumen

La delineación exacta de la próstata, las vesículas seminales, la vejiga y el recto es un paso fundamental para el planeamiento de procedimientos de radioterapia. Protocolos modernos han incluido la delineación de los organos pélvicos en imágenes de resonancia magnética (IRM), como la guía para la irradiación del haz terapéutico sobre el órgano objetivo. Sin embargo, esta tarea es altamente variable intra e inter-experto y puede tomar al rededor de 20 minutos por paciente, incluso para expertos entrenados, convirtiéndose en una carga importante en la mayoría de los servicios de radiología. Métodos automáticos o semi-automáticos podrían mejorar la eficiencia disminuyendo los tiempos medidos mientras se conserva la precisión requerida. Este trabajo presenta una estrategia de segmentación de la próstata completamente automático que selecciona las próstatas más similares con respecto a una imágen de resonancia magnética de prueba y combina las delineaciones asociadas a dichas imagenes para estimar la segmentación de la imágen de prueba. Un análisis multiescala robusto permite establecer el conjunto de las próstatas más parecidas de una base de datos, independiente del protocolo de adquisición. Las imágenes seleccionadas son registradas de forma no rígida con respecto a la imágen de prueba y luego son fusionadas mediante una combinación lineal. El enfoque propuesto fue evaluado utilizando un conjunto público de imágenes de resonancia magnética de pacientes con hiperplasia benigna o con cáncer, con diferentes protocolos de adquisición, esto es 26 externas y 24 endorectales. Este trabajo fue evaluado bajo un esquema *leave-one-out*, cuyos resultados mostraron segmentaciones confiables, obteniendo un DSC promedio de 79%, cuando se compararon los resultados obtenidos con las segmentaciones manuales de expertos.

Palabras Clave: Planeación de la radioterapia, segmentación de la próstata en imagenes de resonancia magnética, enfoques basados en atlas, estrategía de fusión de etiquetas.

Contents

List of Figures

List of Tables

1 Introduction

The prostate is the male reproductive gland responsible for producing the fluid that protects and nourishes the sperm, increasing the spermatozoid spanlife [13]. By a natural process and under the influence of a large quantity of different factors, the prostate may undergo a certain degree of hypertrophy or cancerous lesions. The prostate cancer has become a highly prevalent disease and an important public health problem worldwide, being the second most common cancer in men with about 15 % of the cancers diagnosed in 2012 (approximately 1.1 million men worldwide) [25]. In 2012, 399.964 new cases were reported in Europe and 92.247 deaths were prostate cancer-related [24]. Likewise, in Colombia, about 6.521 new cases and 2.482 prostate cancer-related deaths were discovered in 2014 [52]. Finally, in United States, for 2015 it is estimated 220.000 new cases and 27.540 deaths prostate cancer-related [7]. This disease has triggered a series of public health interventions to improve both the early diagnosis and the patient management. Nowadays, different treatments such as the external beam radiation therapy (ERBT), chemotherapy or surgery constitute the battery upon which the treatment is established, based on the evidence and analysis of the tumor characteristics, nodes and metastases [26]. Currently, the external beam radiation therapy is commonly used as part of any protocol [1] since it has been demonstrated that it reduces the risk of metastasis in early stages [96], while it improves the disease-free survival and relieve the pain in advanced stages [9, 96, 78].

EBRT consists in externally irradiating the target structures (prostate and seminal vesicles) using high-energy x-ray photons during different sessions, delivering different dose quantities according to a pre-established treatment protocol. A first EBRT step is the planning of dose, case in which a computed tomography (CT) is used to delineate the target and organs at risk (OAR) and then design a specific radiation dose delivery map [76, 39]. Such map is usually used to localize the organs of interest in consecutive radiotherapy sessions, under the strong assumption that, with respect to the machine, the organs are located at the same place during the treatment. Recently, Image Guided Radiation Therapy (IGRT) has arisen as a specialized radiotherapy treatment, for which the initial CT is compared with a Cone beam computed tomography (CBCT) image, captured at every sesion, thereby obtaining a better target localization [31, 63] and reducing the toxicity of radiation onto bladder and rectum [51, 43].

In spite of the improvement about target localization in IGRT, supported by CTs delineations, this planning step remains dependent on the expert knowledge with the inherent high intra and inter-expert variability among several delineations [99]. Even worst, the or-

gan delineation on CT volumes is a really difficult task because of the very poor contrast between different soft tissues, which makes organ boundaries indistinguishable, still for a trained expert [37, 67, 83]. Modern protocols have included magnetic resonance imaging (MRI), taking advantage of the high soft tissue contrast and aiming to improve the accuracy of the radiation planning [47]. Overall, the manual delineation carried out over the MRI is typically propagated to the CT by using a registration strategy upon which the dose delivering planning is performed [37]. Although visualization of soft tissues is much better in MRI, nonetheless it is a considerable burden on the workflow of any radiotherapy service, around 20 to 40 minutes per patient [20]). Again, the inter and intra-expert variability is a crucial issue in terms of attention of a real patient [23]. In consequence, reliable and reproducible (semi)-automatic segmentation techniques have an important role in this problem, but they have to cope with a certain number of challenges: 1) the natural variability of organ shape structure [86, 88, 39, 102], 2) the continuous change of physiological states,which resulting in different representations of pixel distribution [18], 3) some prostate regions like the apex remain very blurred [57], 4) the large prostate deformation during MRI endorectal coil (ERC) acquisition [17, 48, 86] and 5) intensity artifacts surrounding the ERC, called near-field effect [4].

Several strategies that segment the prostate in MRI, have been reported, usually using structural and appearance prior information from volume delineations. The prior information is commonly used in strategies such as the statistical shape models, machine learning approaches and atlas based methods. Statistical models use a set of organ observations to construct a statistical organ prior [97] and the most probable organ shape is selected using a customized cost function. These methods are highly dependent on the cost function definition and their accuracy is limited because of the dependency on the available set of samples to deal with the shape variability. Likewise, machine learning techniques try the segmentation as a classification problem, for which a set of image features allows to differentiate between the target organ and the background [27]. However, most of these selected features are global estimators with no spatial information, for instance occurrence descriptors, whose performance is dependent on their invariance, a hard task in such noisy images. Atlas based approaches are still the most often used framework, given the particular advantages to model prior information from a reduced similarity space of samples. Currently, there exist many different applications for which atlas-based approaches have shown competitive results [43, 88, 62]. This atlas-framework builts the prior shape from a set of reduced samples selected according to a similarity criterion. Hence, a main component of these strategies is the cost function metric that allows to statistically narrow the space of samples, while remaining flexible enough to represent the space from different kind of features. The success of such strategies is however highly dependant on this measure, that is commonly defined using appearance features, organ morphology, region identification or specific patterns captured from expert medical knowledge.

1.1 Prostate segmentation strategies on magnetic resonance images

The delineation of the prostate and organs at risk during the IGRT planning is a fundamental step to setting up the irradiation dose during consecutive sessions [105, 65]. Different computational strategies have been proposed in the state-of-the-art to automatically segment organs of interest in image sequences, almost always conserving a relative relationship between the accuracy and the computational time to obtain reliable results [87, 43, 60, 57]. However, many challenges remain open because the natural shape variability, the common fuzzy organ edges and the inclusion of diverse acquisition protocols [86, 88, 39, 102, 57, 17, 48, 86]. In this section is presented a deeply description and analysis of the most relevant computational approaches proposed to segment target structures and organs at risk, including a classification of such strategies according to prior shape modelling and the definition of likelihood rules. In general, most proposed approaches use prior knowledge about the organ of interest that allow to adjust particular shapes in new images by appearance descriptors and machine learning techniques. Four set of methods are described according to prior shape modeling and the definition of likelihood rules to warp this geometrical information to new images. A first group considers statistical shape priors, typically adjusted with low level image features (section 1.1.1). A second group describes the atlas based approaches, that for a new image associate a prior shape obtained from the most similar samples in a MRI population (section 1.1.2). In addition, a third group gathers deformable models and iterative warping techniques (section 1.1.3). Finally, it is described the machine learning methods which try the segmentation as a classification problem to distinguish between the organ of interest and the background (section 1.1.4).
Computational approaches typically take advantage of prior information to better estimate geometry and localization of the organ of interest. Such information is based on oncologist shape delineations. The analyzed strategies were grouped according to the dependence on the prior information and how this representation is warped to each new image, as illistrated in Figure **1-1**. In the following sections are discussed each of these groups.

1.1.1 Statistical Shape Models

Statistical shape models (SSM) are one of the most useful strategies for prostate segmentation, in which a prior shape representation is learned from a set of manual delineations and then such model is coupled with target images [35, 3, 39, 70, 81, 38, 74]. To built the learned shape model, the delineation samples are firstly aligned to be invariant under transformations such as translation, rotation and scaling, and then a principal component analysis (PCA) is used to obtain a statistical shape representation of uncorrelated principal shape components from the set of correlated delineations [10, 14]. The PCA transformation allows to obtain the mean shape $\overline{x}$ and the principal shape variations Pb, where P are the first eigenvectors of

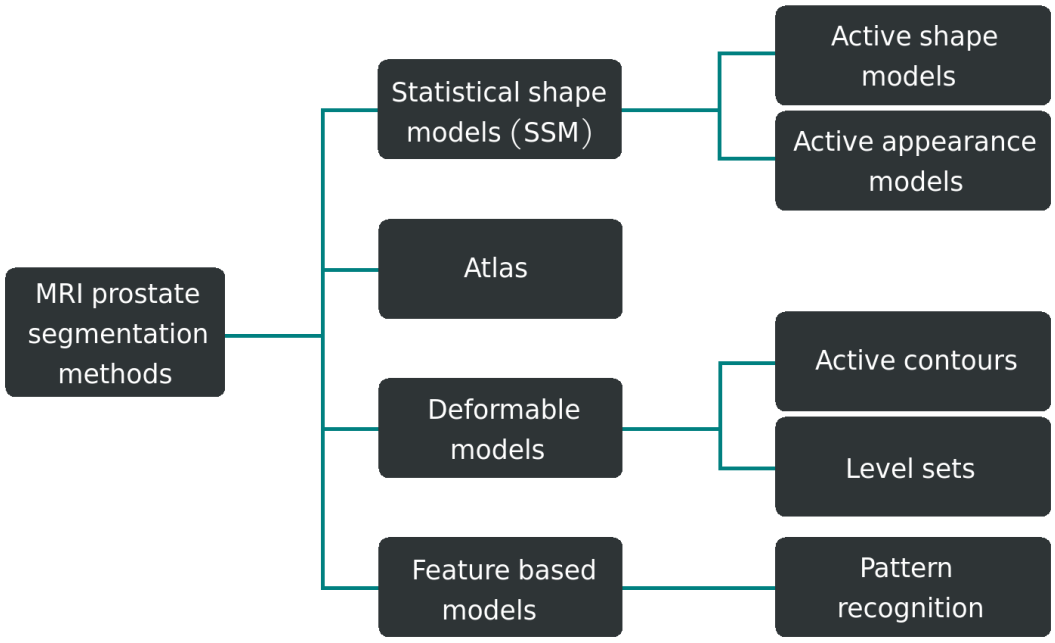

Figure 1-1: Classification of state-of-art strategies. Although in almost all strategies proposed in the literature the prior delineation is fundamental component, each author have proposed different strategies to model this information and also have been proposed different descriptors to extract relevant features about the organs of interest.

covariance matrix and b are the shape model parameters [33, 22]. From this representation is then possible to built a set of shapes with different levels of variance, as $x \approx \overline{x} + Pb$, under a gaussian distribution hypothesis, as seen in Figure **1-2**. Although this strategy has been widely used in many applications, the anatomical variability representation remains limited. Other approaches have tried to cover the shape variability with more sophisticated strategies, for instance, Roweis *et al.* [84] proposed a representation by using an expectation maximization to learn the principal variations. This approach is inherently limited because the accuracy of the representation depends on the initialization parameters, and the rate of convergence in some cases is critical. Prior shapes have also been modelled from Independent component analysis (ICA), by minimizing the statistical dependence between the basis vectors, and therefore maximizing the sparsity [82, 58]. However, this representation many times lost local variability of the structure of interest because the induced sparsity property, which in many cases result fundamental to adjust new shapes. In addition, the dimensionality reduction given by the ICA is not ordered, reason why further algorithms are required to perform vector sorting and discard those that describe noise. Likewise, medial or skeleton models have been used to reduce the shape dimensionality by representing the object using only center lines and corresponding radii collections [8, 90]. However, these

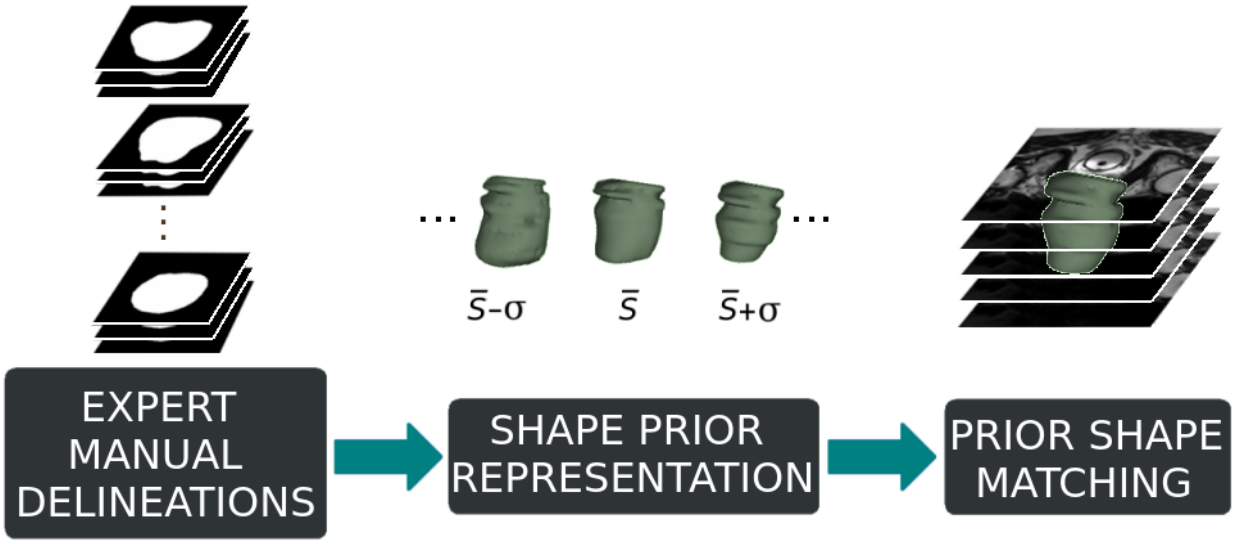

Figure 1-2: Statistical shape models. A set of shapes with different levels of variance is built using expert delineations. Prior shape matching is performed by user interaction or automatic methods.

approaches can fail to detect and identify the skeleton geometries of complex shapes like the organs.

Further strategies have been focused on mapping the prior representation with the target in the image space. This process is performed using local intensity similarity search algorithms that require an initial estimation by user interaction. In these strategies, the expert intervention may introduce inter-observer variability and high time consumption [80]. Alternative approaches have worked in the shape initialization task, by using histogram matching, affine registration with an atlas [41] and evolutionary algorithms (EA) [36]. Such strategies remain with some mistakes for shape initialization because of image noise, intensity variability in a population and artifacts used in clinic (e.g. gold markers) can alter the image appearance.

Alternatively, Active shape models (ASM) [93] couple appearance and shape statistical representations learned from a training database. Such representations are characterized around of a set of landmarks localized close to of the edges of shape delineations. This coupled shape model is then deformed to a new image according to a cost function that locally searches intensity similarities [35]. The cost function is generally expressed as a Mahalanobis distance in the image space that takes into account data correlation and it is invariant to scale [92, 66]. Other metrics have been proposed as an external and internal energy relationship. In this case, the internal energy preserves the smoothness of the contours while the external propagates the deformable model towards a boundary, preserving in this way the shape compactness and coherence [86, 56, 18]. Despite the active shape models incorporate texture information, in many cases these strategies are very sensitive to model initialization

and sometimes fail to converge to the desired edges because of the sparse landmarks correspondence [80]. For automatic shape initialization have been proposed different strategies based on classifiers that localize the region with major probability to contain the prostate, for instance: boosted classifier [56], bayesian methods [15] and k-means clustering [80].
Otherwise, in Active appearance models (AAM) [94] the whole bounded prostate region is fully characterized by its appearance and then coupled with statistical shape models, which combined with search strategies allows to map the learned model to a new image. In this case, the model combines shape and appearance models into a linear system as a compact feature descriptor. In prostate applications, the appearance model has been characterized from texture representation [59, 97, 35] with stable result in a limited group of images, however the accuracy of the method is contrasted with the computational cost. Ghose *et al.* [87] propose a AAM variation to reduce the computation cost, in which the deformation process is carried out by the approximation of Haar wavelet transform coefficients instead of using the raw intensities.

1.1.2 Atlas

Atlas approaches arise as a powerful alternative for prostate segmentation, in which a set of labeled atlases and a similarity criterion allow to pick the most likely shapes for a new unlabeled image. In such strategies, the whole atlas dataset is firstly aligned and warped w.r.t the new image by using classical rigid and nonrigid registration techniques. Typically, rigid registration strategies are used to set a common reference space [71] and non-rigid registration techniques allow to warp the atlases to unlabeled images, such as free-form deformation (FFD) [19] and demons algorithms [95]. According to the number of atlases used to estimate the segmentation, these strategies can be considered as *single* (the most similar atlas is warped to the new image) or *multi atlas* approaches (a set of weighted atlases contributes to estimate the new segmentation). Single-atlas based approaches missed the natural high anatomical variability even when a close appearance similarity is established between two MRI samples. For this reason, it is most common to cover the anatomical shape variability by fusing different atlas segmentations from a local analysis, as depicted in Figure **1-3**.
Once the atlases are warped w.r.t. the new image, a set of the most similar atlases is selected to limit the population of samples and built coherent shape priors for organ segmentation. Several similarity metrics have been proposed to select the most likely atlases according to local appearance characterization. For instance, sum of squared differences (SSD) performs a per-pixel comparison assuming a perfect alignment between the two images [61]. In contrast, the normalized cross correlation (CC) [44, 75] convolves both images by measuring the degree of interdepency from a covariance matrix at a intensity level. The drawback of such techniques lies in simple intensity comparison, which in many of the cases results noisy. On the other hand, mutual information (MI) [45] measure the degree of dependency between

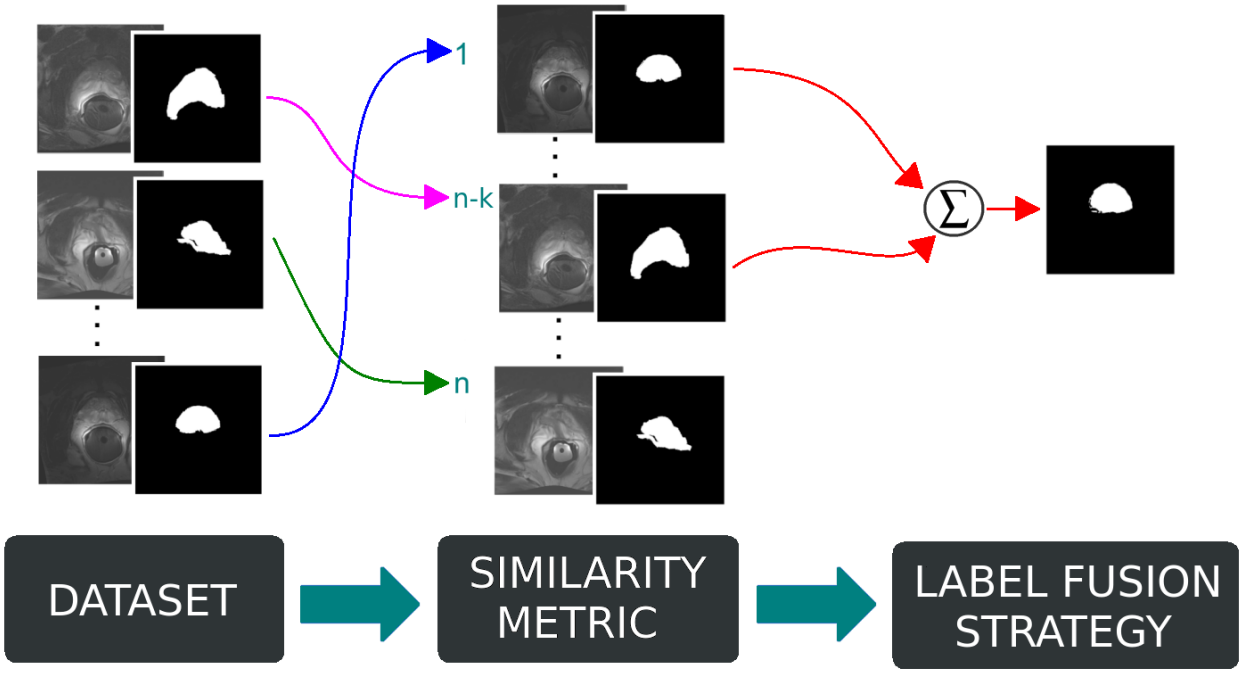

Figure 1-3: Atlas-based approach. A set of similar prostate MRIs are selected based on a similarity criterion, whose associated expert delineations are then combined to obtain the segmentation for a new image.

two images by the joint intensity distribution. This metric is adaptively computed under a stochastic gradient descent method. An additional variation of this approaches named the Normalized mutual information (NMI) results less sensitive to changes in overlap by using the joint entropy to normalized the measure [12, 34, 88]. Such similarity metrics have allowed to reduce the high inter-individual variability regard to the structure of interest and therefore the computational time by not using the whole dataset to built the shape prior. However, the drawback of such techniques lies in the use of classical intensity comparisons, that specially for medical imaging, result in weak and noisy information because adjacent structures may have similar intensity distributions with the target organ boundary.

Additionally, atlas based approaches have focused their attention on defining a proper rule to fuse the most likely atlases and built a shape segmentation on the new image. The majority voting (VOTE) method [42] defines the segmentation as a pixel label agreement. This strategy is highly dependent on an accurate non-rigid registration. Likewise, Litjens et al. [29] proposed an iterative label fusion that discards atlases with less similarity, but with a high registration dependency and high computational cost. An additional well known algorithm is STAPLE (Simultaneous truth and performance level estimation) [89], that statistically models a set of atlases as input to recover the hidden label segmentation. This approach is inherently limited since expectation maximization requires a minimal number of atlases

and parameters for initialization. Specifically on prostate segmentation, Klein *et al.* [88] combined the atlases, selected based on NMI, by using VOTE and STAPLE, reporting large errors at prostate-bladder boundary. A more sophisticated approach proposed by Dowling *et al.* [43] firstly introduced a preprocessing step and then a similarity metric based on a mean reciprocal square difference (MRSD), that allows to obtain reliable segmentations.

1.1.3 Deformable models

Alternatively, deformable models typically warp parametric surfaces and adjust them to the MRI prostate contour, as shown in Figure **1-4** [64]. These strategies require a starting seed (point or surface) and a large amount of constraints to fit the model. In terms of automatic initialization, Makni *et al.* [69] used a statistical geometric model as an initial surface, that was deformed following a Bayesian classification criterion. Likewise, Chandra *et al.* [91] proposed an automatic segmentation approach that set an initial shape from a multi-atlas strategy which is deformed from strong regularizations allowing to preserve shape smoothness near to apex.

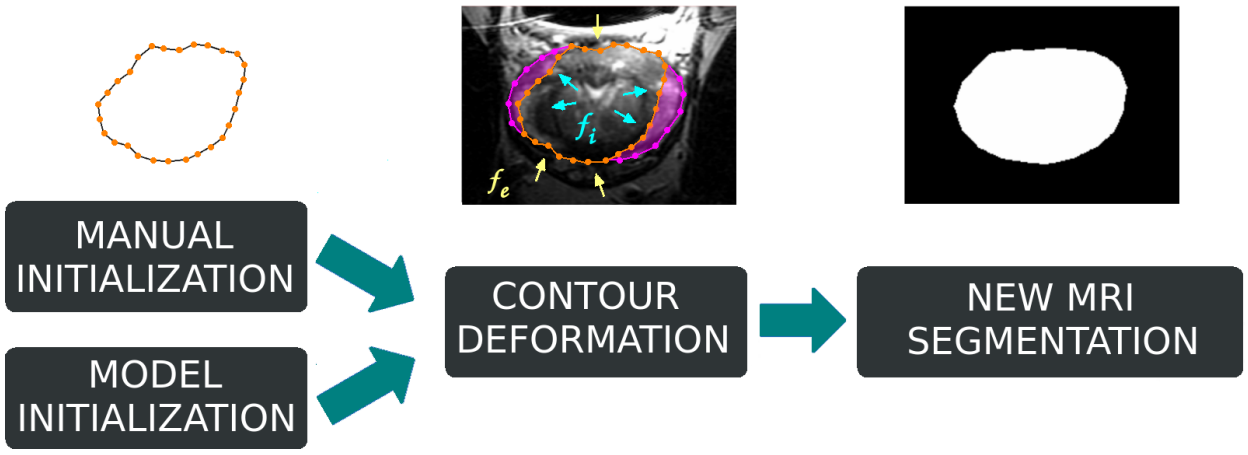

Figure 1-4: Deformable models. An initial seed and a set of constraints are used to warp parametric surfaces and fit them to the target organ contour.

Additionally, deformable models are typically represented as internal and external energies that deform the surface with a global compactness [54, 35, 86]. For instance, Pasquier *et al.* [18] used a seed region-growing method to segment the bladder. However, there are several drawbacks such as the low contrast and therefore indistinguishable edges between the bladder and surrounding organs. Likewise, Garnier *et al.* [11] uses a fast deformable model for bladder segmentation, in which a prior is built from a weighted sum of internal and damping forces that lead a mesh deformation toward the image. This model is computationally expensive because the large number of iterations to adjust complex shapes.

Active contour model (ACM) is one of the most known deformable models, which include a parametric curve that follows the gradient directions of an image target to fit the segmentation [55, 98, 103, 86, 92]. Different approaches have been proposed to overcome manual initialization in ACM, for instance Gao *et al.* [28] used atlas-based approach and Artan *et al.* [101] proposed a graph-based active contour method by using a statistical shape model as an initial shape prior. Active contour models only incorporate edge information and therefore these models may be sensible to noise and present difficulties to be adapted toward complex topologies [104, 98]. In contrast, *level set method* [72, 79] represents the shape contour as a signed function that evolves according to intensity region differences on local neighborhoods [16, 100]. These methods describe topological changes, allowing an efficient splitting and merging of the curve. Nevertheless, this algorithm is sensitive whether the structure of interest has a gap in the boundary.

1.1.4 Feature-based models

Prostate segmentation has been also treated as a classification problem, in which the MRI is projected into an image feature space to characterize different tissues, such as the prostate tissue and the background neighbor tissues that correspond to the bladder and the rectum, as presented in Figure **1-5**. This space, a patchwork of regions, is divided up according to the probability of each feature to be a member of a prostate tissue or the background [86]. In this segmentation strategy, it is typically used supervised learning algorithms that involve phases of training and testing. During training, the MRI features (manually labelled) are learned setting hyperplanes to separate different tissues [85]. Then, a new MRI is segmented by measuring the distance between the features of the new image with the classification model.

Several approaches have been proposed under this machine-learning framework. For instance, Ghose *et al.* [2] used an appearance and spatial patch-based characterization of different tissues, constructing a multitude of decision trees classifiers from a random decision forest. From this classifier was obtained a coarse patch-based prostate segmentation that was refined by a classical level sets propagation. This approach achieved reliable segmentations but manual initialization is required to define the first and last prostate slices.

A more sophisticated approach was proposed by Litjens *et al.* [27], under a multi-feature space that includes geometry, intensity and texture features. The geometry is related with specific salient anatomical positions relative to the organ positions, while the intensity is used to compute the apparent diffusion coefficient (ADC) in each voxel. Finally, texture information is modelled as the homogeneity and correlation using the co-occurrence matrix, histogram information, entropy and texture strength features. A linear discriminant classifier was used under such multidimensional feature space to separate central gland and peripheral prostate zone. Although this approach showed reliable segmentations for the central gland, the peripheral zone remains very challenge because in this zone the tissue is very thin.

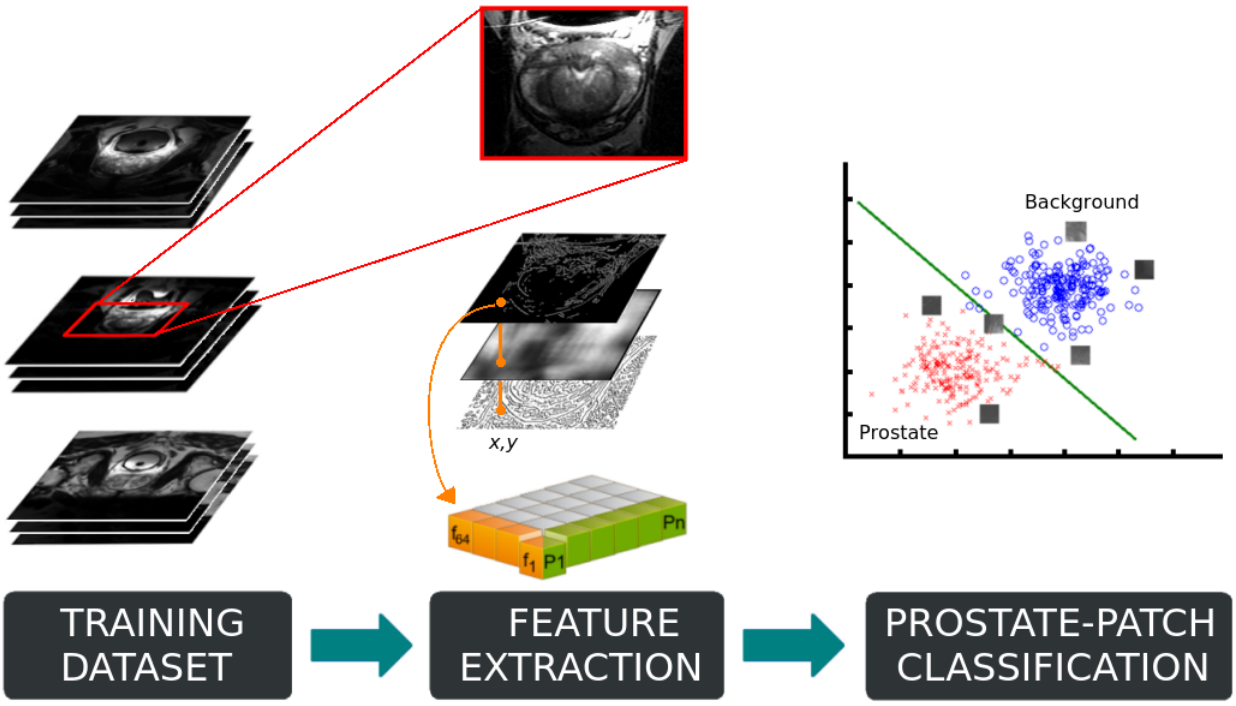

Figure 1-5: Feature-based model. A set of features extracted from MR training images are used to built a classification model that is then used to segment the prostate.

1.2 Contributions and Academic products

This thesis introduces an automatic atlas-based strategy that segments the prostate from MRI sequences, captured during radiotherapy planning. Two main contributions are proposed in this work: a novel similarity metric to narrow the MRI samples and a robust strategy to linearly combine the expert delineations of such subset of MRI samples. For the computation of the similarity metric, the test image and every template in the database are firstly represented in a multi-scale salient point space, in which a reduced set of points allows to describe the region of interest. The main advantage of this representation is the scale and rotation invariance properties that allow a more robust matching between each pair of images. In such multi-scale space, the proposed similarity metric is defined as the occurrence of the SURF points matched using a nearest neighbor algorithm and regularized by the total number of points detected in each RoI. This similarity metric allows to reduce the set of prior-samples in the database, preserving the organ variability but discarding the outliers that have not contribution. Additionally, the multiscale salient point representation allows to recover the most similar templates, independently of the particular MRI capturing modality i.e. external and endorectal coil.

A second contribution, the linear combination of prior delinations, as a set of similar tem-

plates that were previously selected with the similar multiscale criterium, are fussed to estimate the prostate segmentation. For so doing, each selected template is non-rigid registered towards the target, together with the expert associated delineation. Then, a patch-based analysis is performed to estimate the local contribution of each template to the target according to an appearance-similarity rule. This fusion strategy takes advantage of the patient shape variability and shows more reliable results when comparing with the expert manual segmentations. The results of this work were published in:

- **Charlens Álvarez**, Fabio Martínez and Eduardo Romero. *A novel atlas-based approach for MRI prostate segmentation using multiscale points of interest.* Proceedings of the International Seminar on Medical Information Processing and Analysis, SIPAIM 2013, November 11-14, 2013. Ciudad de México, México.
- **Charlens Álvarez**, Fabio Martínez and Eduardo Romero. *An automatic multi-atlas prostate segmentation in MRI using a multiscale representation and a label fusion strategy.* Proceedings of the International Seminar on Medical Information Processing and Analysis, SIPAIM 2014, October 14-16, 2014. Cartagena, Colombia.

1.3 Thesis outline

The remaining chapters of this thesis are organized as follows:

- ***Chapter 2: A novel atlas-based approach for MRI prostate segmentation using multiscale points of interest.*** This chapter presents a prostate segmentation strategy under which a novel multiscale similarity metric allowed to select the most similar template, whose expert segmentation, non-rigidly registered, corresponds to the segmentation for the unlabeled MRI. The proposed strategy demonstrated to be robust to natural high prostate shape and MRI variability, including the fact of mixing up images from different acquisition protocols.
- ***Chapter 3: An automatic multi-atlas prostate segmentation in MRI using a multiscale representation and a label fusion strategy.*** This chapter introduces a multi-atlas strategy for prostate segmentation, taking as advantage of the variability of anatomical structures. Under this strategy, the proposed similarity metric allows to retrieve a set of the most similar templates and a patch-based strategy allows to estimate a statistical prior representation. This framework showed more reliable segmentations when comparing with manual delineations performed by experts.
- ***Chapter 4: Conclusions and Perspectives.*** This final chapter presents the main conclusions of the proposed work, highlighting the main contributions achieved and its impact in the research area. In addition, it depicts some of the future research directions and perspectives promoted by this thesis.

2 A novel atlas-based approach for MRI prostate segmentation using multiscale points of interest

This chapter presents a robust multi-scale similarity analysis in an automatic atlas-based segmentation strategy to select the most probable template from a database. Once that probable template is selected, the associated segmentation is non-rigidly registered to the new MRI. Results show that the method produces reliable segmentations, obtaining an average dice coefficient of 72% when comparing with the expert manual segmentation under a leave-one-out scheme with the training database. *The complete content of this chapter has been published as a research article in the proceedings of* ***9th International Seminar on Medical Information Processing and Analysis*** *(see [5]).*

2.1 Introduction

External beam radiotherapy (EBRT) is the most common treatment for prostate cancer [1]. In such a procedure, a prescribed dose of radiation is applied to the gland tissue, provided that the target volume has been delimited using a manual delineation of the organ in computer tomography images (CT). Besides of the large anatomical variations of the prostate shape, the prostate and its neighboring organs are mostly composed of connective tissues that, when imaged, show poor contrast and then are visually indistinguishable. Currently, new EBRT protocols simultaneously include pelvic CT and MRI captures so that a manual delineation over the MRI is propagated to the CT, improving thereby the accuracy of the radiation planning. Yet visualization of smooth tissues is much better in MRI images, manual delineation nonetheless takes a considerable time (around 20 to 40 minutes to delineate each image) and inevitably introduces high intra and inter expert variability [23, 99]. In consequence, reliable, and reproducible (semi)-automatic segmentation techniques are appealing in this context. Several problems may arise from such automatic methods: 1) the natural shape variability [88], 2) fuzzy borders between neighboring organs [57] and 3) a large prostate deformation when acquiring the image, specifically in MRI endorectal coil (ERC) scans produced by the probe (which is removed during radiation treatment) [48].
Several strategies have been proposed to segment the prostate in MRI, principally using structural and appearance prior information, namely statistical shape models, machine learn-

ing approaches and atlas based methods. Statistical models use a set of organ observations to match an statistical organ prior [97], which is mapped to the space of MRI observations under a customized cost function. These methods however are highly dependent on the cost function definition and their accuracy is limited since they depend on the available number of samples to build up a consistent shape model. Likewise, machine learning techniques try the segmentation as a classification problem, case in which a set of features is set to robustly represent each organ of interest [27]. However, most selected features are global estimators with no spatial information whose performance is dependent on their invariance, a hard task in such noisy images.

The atlas based approaches are still the most frequently applied methodological framework. The general pipeline consists in selecting the prostate shape with the most probable template and register the associated segmentation to the new MRI [62, 88]. Although atlas-based approaches may provide prior structural information, a high inter-individual variability and registration errors can hamper the segmentation. A main step in such approaches is the selection of the most similar templates among a set of prostates, which requires the definition of a similarity measure. An stand out atlas based approach was proposed by Klein et al [88], for which the template selection was performed by using the normalized mutual information (NMI) as similarity index. This metric is nevertheless highly dependant on an accurate rigid registration for it requires to measure the correlation between the same overlapped anatomical structures. Gao [77] proposed to start by splitting external and endorectal coil MRI to reduce the search space. The method uses an intensity regional cost function to select the most probable template, however the result is highly noisy for it uses exclusively intensity values without any anatomical reference.

The main contribution of this work is a novel multiscale similarity metric, under which a prostate candidate is associated with the more similar templates in a database. The method starts by selecting a region of interest (RoI) around the associated segmentation of each template. This RoI is superimposed to the new MRI and used as reference frame, within which, the SURF, a multiresolution transformation, is computed. In such multiresolution SURF space, the set of points of interest are matched by a nearest neighbor algorithm and an euclidean metric, weighted by the correlation of such points, defines a similarity estimation. Finally, the segmentation of the most similar template is propagated by non rigidly registering such template to the new MRI. The rest of this paper is structured as follows: Section 2.2.1 describes alignment and the image pre-processing. Then, in section 2.2.2 is presented RoI extraction and SURF description. In section 2.2.3, the definition of the similarity measure used in the propose method is described. Section 2.2.4 describes the non-rigid registration step and section 2.2.5 present the experimental setup. Finally the evaluation and results obtained by our approach are shown in section 2.3 and the last section concludes with a discussion and possible future work.

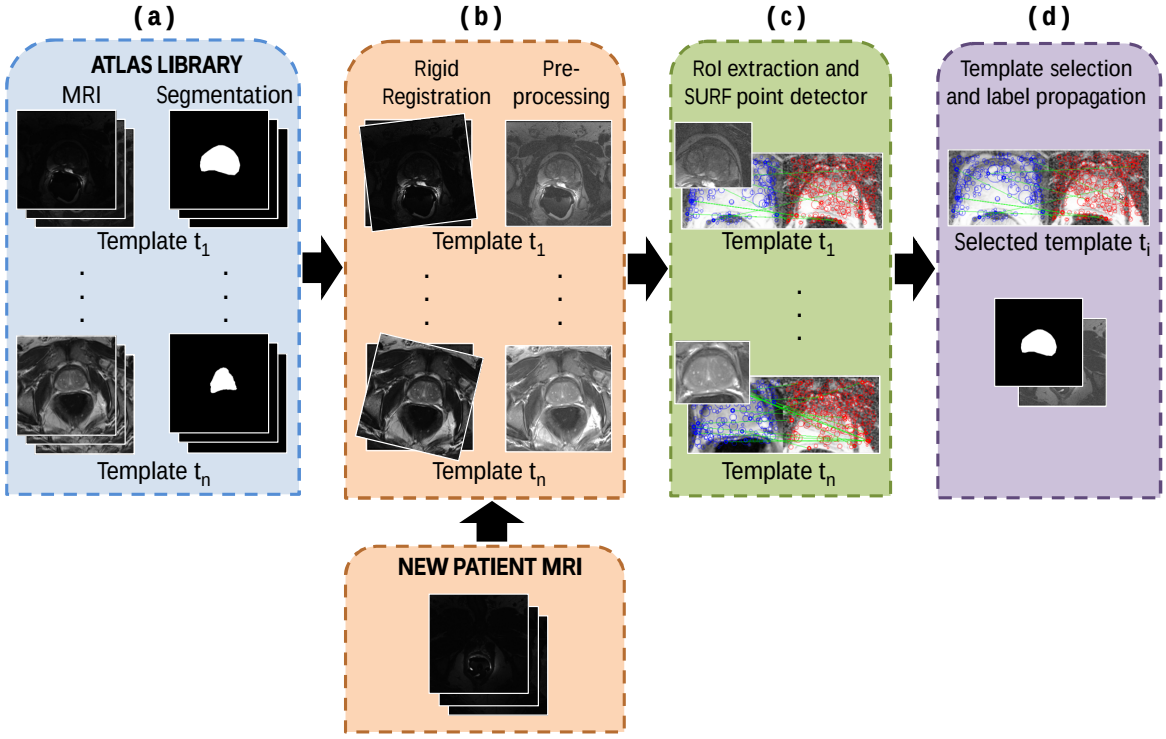

Figure 2-1: The pipeline of the proposed approach. (a) a MRI atlas library is built, each of the prostates is already segmented. (b) the atlas library is aligned w.r.t the new image. Then, the previously determined RoI is superimposed to the new MRI and used as a reference frame within which multiresolution salient points (Surft transform) are calculated (c). Finally, the most similar template is set as the larger number of correspondences between any of the templates and the prostate candidate (d). Selected segmentation is then propagated by non-rigid registration

2.2 Materials and methods

Under an atlas based framework, the proposed approach is able to find the most similar template of a new MRI using a slice-wise multiscale analysis. Firstly, the MRI atlas library was 3D-aligned to a common reference w.r.t the new MRI. Prostate RoIs were computed for each template, using as reference the associated segmentation. Then, they were superimposed to the candidate prostate. A likelihood allowed to find the best geometrical correspondence of a set of computed multiresolution points (SURF) between every atlas and the new MRI. Finally the associated segmentation was 3D-non-rigidly registered to the prostate candidate to obtain a refined segmentation. The proposed method is summarized in Figure **2-1**.

2.2.1 Pre-processing and alignment of Data

In the proposed work, it was codified a prior appearance and shape organ as an atlas-library $\{t_i\}_{i=1}^{n}$ by using a set of n real MRI samples captured from different machines and patients, which have an associated manual prostate delineation s_i. Firstly, it was preprocessed and corrected all samples used to build the atlas in order to remove noise and normalize the high inter-subject intensity variability, leaving each tissue type more uniformly along the dataset [50]. Then, the atlas library was then rigidly registered with the new MRI using a classical "block matching" method [71], thereby ensuring a common reference space. For so doing, a non-local means algorithm [46] was firstly used to remove the acquisition noise, followed by a simple histogram equalization that normalizes intensity contrast of every pelvic tissue. Thus, a set of RoIs with size $\{S_i' = S_i + \xi\}$ were set for the whole set of data, being S_i' the organ segmentation associated to every template t_i and ξ a tolerance value.

2.2.2 Multiresolution MRI Shape Representation

Multiresolution modeling aims to capture structural image information that should somehow conserve a certain coherence among the different scales [53, 49]. In this work, it was obtained a multiresolution representation of each RoI using the Speeded Up Features (SURF) detector and descriptor [32]. SURF, in general terms, offers an invariant image description, allowing a robust representation against illumination, scale and rotation changes. For the proposed approach, the salient multiresolution points compactly describe the prostate and neighbor organs.

For SURF description, a multiresolution image decomposition is firstly carried out by operating a Hessian matrix over the integral image representation, defined as: $I_{\sum}(\mathbf{x})$. In this descriptor, a Hessian matrix is convolved at each specific point X and for each particular scale σ, as:

$$H(X,\sigma) = \begin{bmatrix} L_{xx}(X,\sigma) & L_{xy}(X,\sigma) \\ L_{xy}(X,\sigma) & L_{yy}(X,\sigma) \end{bmatrix} \tag{2-1}$$

A set of salient points are then obtained as the maximum determinant of the Hessian (DoH), as : $|DoH(u)| > t_h$, where t_h is a relevancy threshold. Each point is composed of its associated scale, a unique orientation estimated using the Haar wavelet coefficients and a set of features calculated within its neighbourhood. Finally correlation between salient points of the two prostates, MRI candidate and template, was carried out by a classical fast nearest neighbor algorithm, using the SURF descriptor as point matching criterion [68].

2.2.3 Likelihood measure

A likelihood measure was defined as the manual segmentation that better adjust to the MRI prostate candidate. This similarity measure takes advantage of the spatial relationship

among m matched points from the total k detected points in the MRI prostate candidate and j MRI template points. The per-slice likelihood metric d is defined as:

$$d(\mathbf{X_a}, \mathbf{U_a}) = \|\mathbf{X_a} - \mathbf{U_a}\| + W_a \tag{2-2}$$

where $\mathbf{X_a} = [x_{a1}, x_{a2}, \ldots, x_{am}]$ and $\mathbf{U_a} = [u_{a1}, u_{a2}, \ldots, u_{am}]$ are arranged vectors that contain the set of matched points of each template and the MRI prostate candidate, respectively. In such case, the vector size is m with $m \leq k, j$. The likelihood metric is also regularized as the point detected rate W_a in both RoIs as: $W_i = \frac{|2m-|ak-aj||}{ak+aj}$. A global metric for the two MRI volumes is then a simple average of the computed metric among the L slices, defined as: $sm = \frac{1}{L}\sum_{a=1}^{L} d(\mathbf{X_a}, \mathbf{U_a})$. This metric is only computed in the L slices with prostate segmentation associated in each template.

2.2.4 Shape refinement by structural analysis and non-rigid propagation

From the similarity metric, each template of the atlas library was sorted out using the multiresolution coherence w.r.t the MRI prostate candidate. Then, a reduced set of the most probable templates was selected to build a prostate probability map. This map is constructed by assigning the highest probability to those voxels belonging to the largest number of prostate segmentations. From this structural probability map, the delimited set of templates are compared through an overlapping measure. The more probable segmentation is then assigned to the new MRI. Furthermore, the associated segmentation was selected from a multiresolution analysis but with an structural shape coherence. Finally, two non-rigid registration state-of-the-art techniques were used to locally warp the template image, either free-form deformation (FFD) [19] and the demons [95].

2.2.5 Data

The evaluation of the proposed approach was performed over a public dataset PROMISE12 [30], that consists of 50 MRI cases, 24 of them were acquired with endorectal coil. The dataset just included axial T2-weighted MR pelvic images, acquired to dose planning in radiotherapy treatment. Such dataset included patients with prostatic hyperplasia or prostate cancer. The prostate was manually delineated by an oncologist expert. The dataset is challenged since the cases were acquired from acquisition protocols in diverse clinicals and acquisition scanners. Such fact may produces high inter-slice distance variability (from 0.27 to 0.75) and image resolution (from 256x256 to 512x512). In addition, the data is a multi-center and multi-vendor.

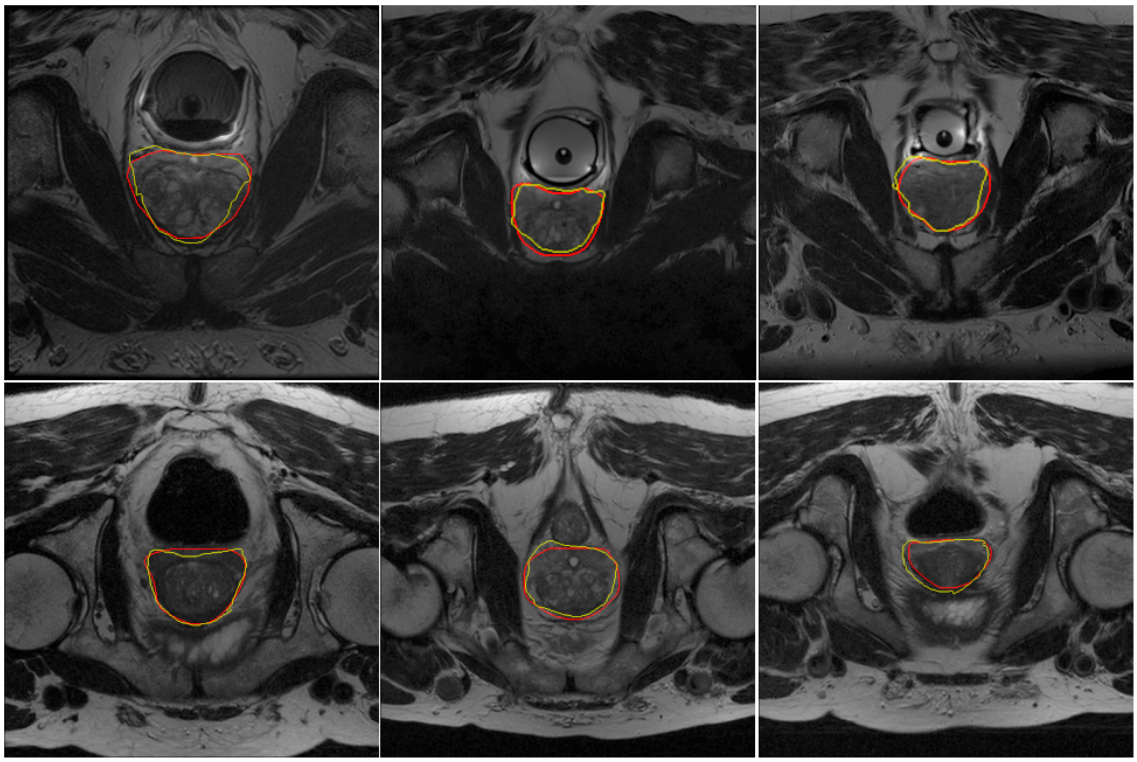

Figure 2-2: Prostate segmentation result using the proposed approach. The comparison of the of the expert segmentation (red) with the obtained by the proposed strategy (yellow). The first line corresponds to three different endorectal coil scans and the second corresponds to external scans.

2.3 Evaluation and Results

The evaluation was performed under a leave-one-out cross validation scheme, each time a different MRI was selected as test while the remaining 49 cases in the dataset were used to build the atlas library. The Figure 2 illustrates the good performance of the method in MRI cases. The red contour corresponds to the result obtained by the presented method and the ground truth is represented by the yellow contour, reaching in some cases perfect overlap. As expected, failures are mainly present in apical slices because of the fuzzy borders of the prostate.

Quantitative evaluation was performed using classical metrics described in the literature: Dice score (DSC) measure and Hausdorff distance (HD). An overlap DSC measure is defined as: $DSC(A,B) = \frac{2(A \cap B)}{A+B}$, where A and B represent the obtained area and the expert ground truth, respectively. On the other hand, the Hausdorff measure $H(A,B)$ computes the maximum distance between two sets of points as $\max(h(A,B), h(B,A))$ and $h(A,B) = \max_{a \in A} \min_{b \in B} \|a-b\|_2^2$. In this case, each set of points represents the organ surface. This

measure allows to indirectly assess the compactness of the segmentation.
The table **2-1** summarizes the performance obtained by the proposed approach. As baseline it was taken the work proposed by Dowling, et al [40], since such approach also uses atlas strategy. Although the performance of the proposed approach result statisticallly similar, the complete framework of the baseline is much more complex using a multi-atlas approach and a fusion label step to get the final segmentation. Currently, state-of-the-art approaches obtain better scores but a manual initialization is required. Classical approaches as the Level set approach [2] or Active appearance models [97] have been also tested to try to solve this problem. However, such methods also fail on Apex and Base prostate warping out the segmentation of the organ.

Table 2-1: Quantitative results on the training data. The mean and standard deviation of the respective measure from 50 experiments in a live-one-out scheme.

Segmentation	**DSC (mean + sd)**	**HD**
Proposed method	0.72 ± 0.13	12.61 ± 5.6
Atlas approach [40]	0.73 ± 0.13	–

The proposed approach is a fully automatic strategy and also it is able to work independently of the acquisition modality i.e. without any previous classification of external or endorectal coil MRI. Also, under an specific analysis over the RoI by relying in the segmentations performed by the oncologist over the data in the library was possible to characterize the prostate and the closer tissues allowing to find the most similar configuration between the new MRI and each atlas-template.

2.4 Conclusion

A new methodology for segmenting the prostate in MRI was proposed based on multiresolution analysis to associate a manual prostate segmentation to a new MRI. The proposed method takes advantage of both the interindividual shape variation and intra-individual salient points representation. The method is robust to natural high prostate shape and MRI variability, including the fact of mixing up images from different modalities. The results of this paper suggest this metrics is very robust, not only because it is able to compare multimodal images but rather since such a simple strategy reaches similar results to those obtained by much more complicated frameworks used in the state-of-the-art. Future work includes the extension of the proposed approach to segment the organs at risk, such as bladder and rectum. Another future work includes validation with a larger data set.

3 An automatic multi-atlas prostate segmentation in MRI using a multiscale representation and a label fusion strategy

This chapter presents a fully automatic atlas-based segmentation strategy that selects a set of more similar templates for a new MRI using a robust multi-scale SURF analysis. Then a new segmentation is achieved by a linear combination of the selected templates, which are previously non-rigidly registered towards the new image. The proposed method shows reliable segmentations, obtaining an average dice coefficient of 79%, when comparing with the expert manual segmentation, under a leave-one-out scheme with the training database. *A complete version of this chapter has been accepted for publication as a research article in the proceedings of* ***10th International Seminar on Medical Information Processing and Analysis*** *(see [6].*

3.1 Introduction

Prostate cancer has become a highly prevalent disease and an important public health problem [25], usually treated by external beam radiotherapy (EBRT) [1]. In EBRT, a prescribed radiation dose is applied to the gland tissue, reason why it is crucial to accurately segment the prostate volume and surrounding organs. Currently, EBRT protocols include manual delineation of MRI prostate sequences, estimations that are then used as templates in CT images. However, manual delineations are a considerable burden (each around 20 to 40 minutes) and highly within and inter-expert variable [23]. In consequence, reliable and reproducible (semi)-automatic segmentation techniques have to cope with a certain number of challenges: 1) the natural shape variability [88], 2) fuzzy borders between neighboring organs [57] and 3) the large prostate deformation when acquiring the image [48].
Several strategies have been proposed to segment the prostate in MRI, mainly using structural and appearance prior information such as statistical shape models, machine learning approaches and atlas based methods, which are the most frequently applied. In such case, a set of labelled atlases and a similarity criterion allow to pick the most likely segmentation

for a new test image [88]. Multi-atlas strategies commonly include label fusion methods to estimate the most probable segmentation. For instance, the majority voting [42] sets a label by a pixel-to-pixel atlases agreement. On the other hand, Litjens et al. [29] proposed an iterative label fusion that discards atlases with less similarity, but with a high registration dependency and high computationally cost. Likewise, the STAPLE algorithm (Simultaneous truth and performance level estimation) [89], statistically models a set of atlases as input to recover the hidden label segmentation. This approach is inherently limited since expectation maximization requires a minimal number of atlases and parameters for initialization.

In this work, an automatic prostate segmentation method is presented. The approach is constructed upon a novel SURF-based similarity metric that retrieves alike prostate MRI images from the dataset, which are then non-rigidly registered toward a new MRI. This strategy is complemented by a label fusion process, consisting in a linear combination of weighted patches from the selected prostates, obtaining a statistical representative of the set of registered prostates.

3.2 Materials and methods

Given a new MRI, the proposed approach automatically selects, from a training bank of samples, a subset of similar prostates using a robust multi-scale analysis (Figure **3-1**(a) and further description in sections 3.2.1 and 3.2.2). The selected prostates are non-rigidly registered to the new MRI and a final segmentation is constructed by linearly combining weighted patches from the set of similar prostates(Figure **3-1**(b) and further description in section 3.2.3).

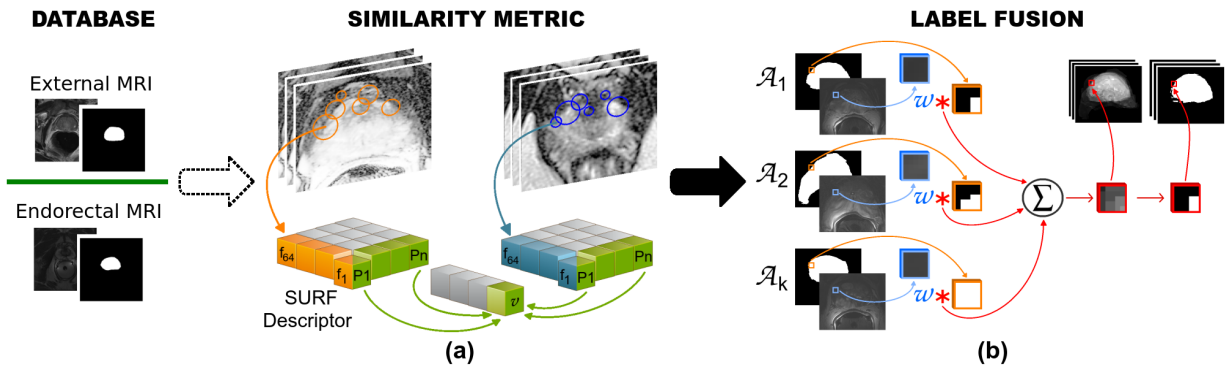

Figure 3-1: Pipeline of the proposed approach. In (a), it was selected a subset of similar prostates from the database under a multi-scale shape representation. In (b), the selected prostates are non-rigidly registered and then by using a patch-based strategy are linearly combined to get the final segmentation.

3.2.1 Pre-processing and alignment of Data

As a first step, the dataset is pre-processed using histogram equalization to normalize the high inter-subject intensity variability. The dataset is then rigidly registered with respect to the target MRI prostate using a classical "block matching" method and so ensuring a common reference space. A region of interest (RoI) is then defined by enclosing the prostate.

3.2.2 The similarity metric from a multiscale MRI shape representation

The similarity metric aims to select the manual prostate delineations that better adjust the target image. For doing so, over the aligned dataset w.r.t the new image, the RoIs in both each dataset image and the new MRI are characterized by the Speeded Up Features (SURF) detector and descriptor [32]. This descriptor is robust to illumination, scale and rotation changes [32]. The SURF descriptor convolves the Hessian matrix over an Integral image representation, determining those points with larger multiscale variability through different scales.

$$H(X,\sigma) = \begin{bmatrix} L_{xx}(X,\sigma) & L_{xy}(X,\sigma) \\ L_{xy}(X,\sigma) & L_{yy}(X,\sigma) \end{bmatrix} \tag{3-1}$$

A set of salient points are defined as the points with maximum determinant of the Hessian (DoH) through different scales. For each salient point, available information includes the scale at which the point was obtained, orientation estimated using the Haar wavelet coefficients and the gradients computed within the point neighbourhood. In addition, the descriptor was modified to include a structural coherence weight: the distance between the found point and the manual delineation boundary. Afterwards, a matching between salient points in both images was computed by a classical fast nearest neighbor algorithm.
The final per-slice metric d is then defined as: $d(\mathbf{X_a}, \mathbf{U_a}) = \|\mathbf{X_a} - \mathbf{U_a}\| + W_a$, where $\mathbf{X_a} = [x_{a1}, \ldots, x_{am}]$ and $\mathbf{U_a} = [u_{a1}, \ldots, u_{am}]$ are arranged vectors that contain the set of matched points of each prostate and the new MRI, respectively. The proposed similarity metric is also regularized by the point detected rate W_a in both RoIs, defined as: $W_a = \frac{|2m - |ak - aj||}{ak + aj}$, where m is the number of matched points, and k, j are the number of points found in the database and target ROI prostates, respectively. A global metric for the two MRI volumes is then a simple average of the computed metric among the L slices, defined as: $sm = \frac{1}{L}\sum_{a=1}^{L} d(\mathbf{X_a}, \mathbf{U_a})$.
This metric is only computed over the L slices with prostate segmentation. The proposed measure assume a 3D organ correspondence of the multiscale salient points, since the whole atlas and the new MRI are in the same reference space because the previous rigid transformation.

3.2.3 Shape estimation: the label fusion strategy

Once a set of selected prostates is collected, an estimated segmentation of the target MRI is built as a linear combination of these prostates by using a patch-based strategy, consisting in locally weighting each prostate patch by its similarity. First, the selected prostates are non-rigidly registered to the new MRI prostate using the free-form deformation algorithm (FFD). Afterwards, in a slice-wise analysis, for all patches surrounding pixel x_i in the target MRI, the final label is estimated by using a label fusion function $\varphi(x_i)$ of the N deformed segmentations, as follows:

$$\varphi(x_i) = \frac{\sum_{k=1}^{N} w(P_t(x_i), P_{A_k}(x_i)) L_{A_k}(x_i)}{\sum_{k=1}^{N} w(P_t(x_i), P_{A_k}(x_i))} \tag{3-2}$$

where $P_t(x_i)$ is an intensity patch from the target image centered at the x_i pixel, $P_{A_k}(x_i)$ is an intensity patch from each of the MRI prostates centered at the same x_i pixel, $L_{A_k(x_i)}$ is a patch from each of the delineated prostates, and $w(P_t(x_i), P_{A_k}(x_i))$ is the weight assigned to the $L_{A_k(x_i)}$ by comparing the intensity patches using a non-local means estimator, defined as: $w(P_t(x_i), P_{A_k}(x_i)) = e^{\frac{-\left\|P_t(x_i) - P_{A_k}(x_i)\right\|_2^2}{h}}$, where h is a filtering parameter that allows to control the decay of the exponential function [46].

3.2.4 Data

The evaluation of the proposed approach was performed using a public dataset PROMISE12 [30], composed of 50 MRI cases, 24 of them acquired with endorectal coil. The dataset contains only axial T2-weighted MR pelvic images, acquired for dose planning in radiotherapy treatment. Such dataset includes patients with prostatic hyperplasia or prostate cancer, each manually delineated by an expert oncologist. This dataset is challenging since cases were acquired using protocols from different clinicals and scanners, increasing the high inter-slice distance (from 0.27 to 0.75) and image resolution (from 256x256 to 512x512).

3.3 Evaluation and results

The evaluation was performed under a leave-one-out cross validation scheme, using a dice coefficient (DSC) [21] to measure the segmentation accuracy. Two different label fusion strategies were tested: majority voting, i.e., a pixel-to-pixel atlases agreement and the proposed patch-based strategy. Figure **3-2** illustrates the segmentation results using the majority voting and the patch based approach as label fusion strategies for external and endorectal prostate scans. The red and yellow contours stand for the estimated and expert segmentations respectively, reaching reliable overlapping. As expected, failures are mainly present in apical slices, because of the fuzzy borders of the prostate.

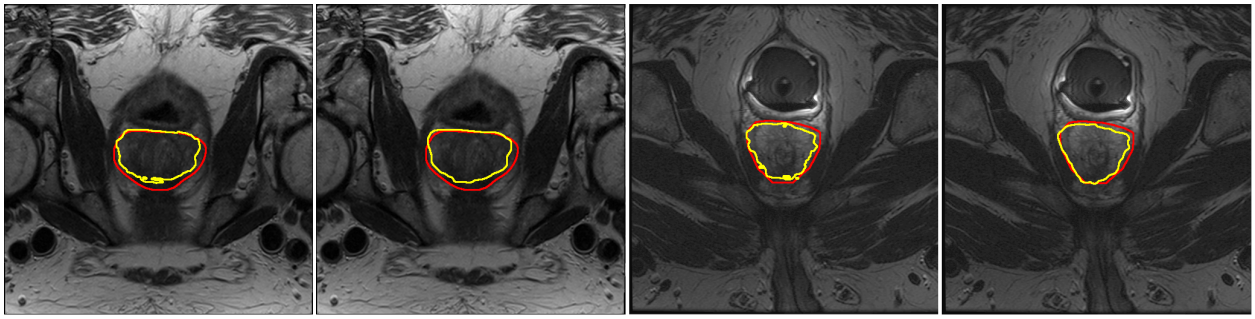

Figure 3-2: Prostate segmentation results using the proposed approach. The comparison of the expert segmentation (red) with the proposed strategy (yellow). Images (a) and (c) stand for the obtained segmentation using majority voting for external and endorectal cases respectively. Images (b) and (d) stand for the obtained segmentation using the proposed patch-based label fusion strategy.

An analysis of two main parameters of the proposed approach was performed: the number of similar atlases and the patch size used for estimating the segmentation. In table **3-1** is shown the segmentation results using different number of atlases with a fixed patch size of 31×31. In average, the optimal number of atlases is 10 (statistically equivalent with 15 atlases), because it shows reliable results, capturing the organ shape variability of the population with efficient time machine.

Table 3-1: Segmentation results of the proposed multi-atlas approach using different number of atlases and a fixed patch size of 31×31

N. of atlas	**DSC (mean $\pm$ sd)**
5	0.67 ± 0.19
10	$\mathbf{0.74 \pm 0.18}$
15	0.73 ± 0.11

In table **3-2** is shown the segmentation results using different patch sizes for the atlas combination. The optimal patch size was of 3×3, showing in general a compact organ segmentation without losing local shape variability. While the patch size is increasing, the resulting segmentation loses local details of the shape.
In Table **3-3**, it was compared the proposed approach with a state-of-the-art multi-atlas strategy [29]. In spite of the obtained DSC for both strategies is quite similar, the proposed approach achieve a robust shape representation from a reduced space of atlases. This point

Table 3-2: Segmentation results of the proposed multi-atlas approach using different patch sizes for atlas combination

N. of atlas	Patch size	DSC (mean ± sd)
10	**3**	**0.79 ± 0.10**
	7	0.78 ± 0.11
	15	0.77 ± 0.11
	31	0.74 ± 0.18
	63	0.37 ± 0.30

allows to obtain reliable segmentations with efficiency in time, a critical issue for real clinical implementation. An additional advantage of the proposed approach is the fully automatic search of the most similar prostates in a mixed dataset, i.e. external and endorectal coil MRI, while the baseline atlas-based approach requires a previous classification of MRI modalities.

Table 3-3: Segmentation results (DSC with the associated standard deviation) of the proposed approach and a state-of-the-art multi-atlas strategy

Segmentation strategy	DSC (mean ± sd)
Proposed approach	**0.79 ± 0.10**
Multi-atlas approach et al. [29]	0.78 ± 0.12

Additionally, Gao et al. [77] proposed a multi-atlas strategy, reporting in average a higher DSC result (0.84). However, this reported DSC was computed withot including individual cases with failling segmentations (DSC less than 0.4). These outlier cases reduce significantly the accuracy of the segmentation and result in totally lost of the shape compactnes, which is a great drawback for the radiotherapy planning task. Likewise, in Ou et al [73] is only reported the DSC of a reduced set of cases (only six cases were taking into account), which is not comparable with our evaluation scheme.

3.4 Conclusion

We have described an automatic multi-atlas approach for segmenting a new prostate MRI. From a multiresolution analysis is selected the most similar atlases and then a linear com-

bination of the associated delineation allows to obtain the new prostate segmentation. The proposed method takes advantage of both the interindividual shape variation and intra-individual salient point representation. We show that by using the proposed metric, the best representative prostates were obtained, independently of the particular capturing modality i.e. external and endorectal coil MRI. Future work includes the method extension to segment the organs at risk, such as bladder and rectum, as well as validation with a larger data set.

4 Conclusions and perspectives

4.1 Conclusions

This thesis has developed and validated a fully automatic atlas-based framework to segment the prostate in magnetic resonance images. A main contribution has introduced a multiscale analysis that characterizes the structure of interest, the prostate gland, by defining a similarity metric that is able to find the most similar prostates in a database. The similarity metric uses prostate salient points, from the image, and medical knowledge, from the expert delineations, to perform the multiscale analysis. Additionally, the segmentation is refined by linearly combining the most similar prostates, i.e., the associated segmentations are split into small patches that are combined with weights that depend on the similarity between the group of similar prostates and the test image at exactly the position of those patches. This fusion strategy takes advantage of the inter-individual shape variation, allowing to estimate a more accurate segmentation.
The proposed framework provides an efficient representation of the prostate organ, setting the most similar prostates independently of the particular MRI acquisiton protocol, an important side advantage that increases the number of prostates in the database. That is to say, with a dataset including external and endorectal MR images, this framework need not require an initial classification of the dataset between external and endorectal scans as many state-of-the-art approaches. The results of this work suggest the proposed framework reaches similar results to those obtained by much more complicated frameworks used in the state-of-the-art.

4.2 Perspectives

This thesis has contributed to the construction of a computational framework for morphometrical analyses of medical images, providing a set of analysis, interpretation and visualization tools that serves as a support for diagnosis, training and research processes. For a physician, the possibility of obtaining quantitative and complementary information about the patient condition, refines the medical management, decreases the diagnostic variability and results in more accurate treatments, impacting directly the patient quality-of-life. Also, compilation and comparison of this knowledge, within different populations, affects positively the development of public and preventative health policies. We expect that the proposed

computational tools, in the future, will contribute to these medical advances. while in the meanwhile, some work must be performed to prepare these tools to be used by medical experts in a daily basis. Some of this work includes.

1. **Extension for segmentating the organs at risk:** External beam radiation therapy uses high levels of radiation to eliminate cancer cells or prevent their growing. The use of medical images has allowed more accurate localization of the prostate structure and therefore has improved the radiotherapy planning. However, in despite of these improvements, there exist risks of toxicity during each radiotherapy procedure over the surrounding organs namely the bladder and the rectum. The toxicity of the radiation consequently yields short and long side effects [7, 13]. Reason why future work includes the extension of the proposed framework to segment the organs at risk.

2. **Performance validation with larger data sets:** Evaluation of the proposed framework has been performed with a public dataset to facilitate comparison with other approaches and their published results. Yet the used dataset shows some differences along the MR images such as multiple centers, multiple MRI device vendors, different acquisition protocols (e.g. external and endorectal) and patients with different pathologies (e.g. benign prostatic hyperplasia and prostate cancer), this dataset does not provide an adequate number of cases as to reach significant statistical conclusions. More accurate and reliable segmentations demand the proposed framework must be exhaustively evaluated in larger data sets.

Bibliography

[1] A. D'Amico, S. Malkowicz D. Schultz K. Blank G. Broderick-J. Tomaszewski A. Renshaw I. Kaplan C. B. ; Wein, A.: Biochemical outcome after radical prostatectomy, external beam radiation therapy, or interstitial radiation therapy for clinically localized prostate cancer. In: *Jama* 280 (1998), p. 969–974

[2] A. Oliver, X. Llado J. Freixenet J.C. Vilanova D. Sidibe-S. Ghose J. M. ; Meriaudeau, F.: A random forest based classification approach to prostate segmentation in mri. In: *Promise Miccai 2012 Grand Challenge on Prostate MR Image Segmentation*, 2012, p. 20–27

[3] A. Srivastava, W. M. ; Liu, X.: Statistical shape analysis: Clustering, learning, and testing. In: *IEEE Transactions on Pattern Analysis and Machine Intelligence* 27(4) (2005), p. 590–602

[4] A. Tsai, W.M. Wells III C.M. Tempany D. Tucker A. Fan W.E.L. G. ; Willsky, A.: A shape-based approach to the segmentation of medical imagery using level sets. In: *IEEE Transactions on medical imaging* 22(2) (2003), p. 137–154

[5] Álvarez, Charlens ; Martínez, Fabio ; Romero, Eduardo: A novel atlas-based approach for MRI prostate segmentation using multiscale points of interest. In: *Proc. SPIE* 8922 (2013), p. 89220O–89220O–D

[6] Álvarez, Charlens ; Martínez, Fabio ; Romero, Eduardo. *An automatic multi-atlas prostate segmentation in MRI using a multiscale representation and a label fusion strategy.* 2015

[7] American Cancer Society. *Cancer Facts & Figures 2015.* Atlanta: American Cancer Society. Available: http://www.cancer.org/. 2015

[8] Blum, H.: Biological shape and visual science (part i). In: *Journal of Theoretical Biology* 38(2) (1973), p. 205–287

[9] Bolla, Michel ; Gonzalez, Dionisio ; Warde, Padraig ; Dubois, Jean B. ; Mirimanoff, René-Olivier ; Storme, Guy ; Bernier, Jacques ; Kuten, Abraham ; Sternberg, Cora ; Gil, Thierry ; Collette, Laurence ; Pierart, Marianne: Improved Survival in Patients with Locally Advanced Prostate Cancer Treated with

Radiotherapy and Goserelin. In: *New England Journal of Medicine* 337 (1997), Nr. 5, p. 295–300. – PMID: 9233866

[10] Bookstein, F.L.: Landmark methods for forms without landmarks: morphometrics of group differences in outline shape. In: *Medical Image Analysis* 1(3) (1997), p. 225–243

[11] C. Garnier, W. K. ; Dillenseger, J.L.: Bladder segmentation in mri images using active region growing model. In: *Engineering in Medicine and Biology Society,EMBC, Annual International Conference of the IEEE*, 2011, p. 5702–5705

[12] C. Studholme, D.L.G. H. ; Hawkes, D.J.: An overlap invariant entropy measure of 3D medical image alignment. In: *Pattern Recognition* 32(1) (1999), p. 71–86

[13] Coakley, Fergus V. ; Hricak, Hedvig: {RADIOLOGIC} {ANATOMY} {OF} {THE} {PROSTATE} GLAND: A {CLINICAL} {APPROACH}. In: *Radiologic Clinics of North America* 38 (2000), Nr. 1, p. 15 – 30. – ISSN 0033–8389

[14] Cootes, T. ; Taylor, C.: Statistical models of appearance for computer vision, 1999

[15] Cosio, F.A.: Automatic initialization of an active shape model of the prostate. In: *Medical Image Analysis* 12(4) (2008), p. 469–483

[16] D. Cremers, M. R. ; Deriche, R.: A review of statistical approaches to level set segmentation: Integrating color, texture, motion and shape. In: *Int. J. Comput. Vision* 72(2) (2007), p. 195–215

[17] D. Flores-Tapia, N. Venugopal B. M. ; Pistorius, S.: Semi automatic mri prostate segmentation based on wavelet multiscale products. In: *Engineering in Medicine and Biology Society, EMBS, 30th Annual International Conference of the IEEE* (2008), p. 3020–3023

[18] D. Pasquier, M. Vermandel J. Rousseau E. L. ; Betrouni, N.: Automatic segmentation of pelvic structures from magnetic resonance images for prostate cancer radiotherapy. In: *International journal of radiation oncology, biology, physics* 68(2) (2007), p. 592–600

[19] D. Rueckert, C. Hayes D. Hill M.O. L. ; Hawkes, D.: Nonrigid registration using free-form deformations: application to breast mr images. In: *Medical Imaging, IEEE Transactions* 18 (8) (1999), p. 712–721

[20] D.C. Collier, M. Amin S. Bilton C. Brooks A. Ryan D. Roniger D. T. ; Starkschall, G.: Assessment of consistency in contouring of normal-tissue anatomic structures. In: *Journal of Applied Clinical Medical Physics* 4(1) (2003), p. 17–24

[21] Dice, L.R.: Measures of the Amount of Ecologic Association Between Species. In: *Ecology* 26 (3) (1945), p. 297–302

[22] Dryden, I.L. ; Mardia, K.V.: Statistical shape analysis. In: *Wiley series in probability and statistics. Wiley, Chichester [u.a.]* (1998)

[23] E. Berthelet, A. Agranovich K. P. ; Currie, T.: Computed tomography determination of prostate volume and maximum dimensions: a study of interobserver variability. In: *Radiotherapy and Oncology* 63 (1) (2002), p. 37–40

[24] Ferlay, J. ; Steliarova-Foucher, E. ; Lortet-Tieulent, J. ; Rosso, S. ; Coebergh, J.W.W. ; Comber, H. ; Forman, D. ; Bray, F.: Cancer incidence and mortality patterns in Europe: Estimates for 40 countries in 2012. In: *European Journal of Cancer* 49 (2013), Nr. 6, p. 1374 – 1403. – ISSN 0959–8049

[25] Ferlay J, Ervik M Dikshit R Eser S Mathers C Rebelo M Parkin DM Forman D Bray F. *GLOBOCAN 2012 v1.0, Cancer Incidence and Mortality Worldwide: IARC CancerBase No. 11.* Lyon, France: International Agency for Research on Cancer. Available: http://globocan.iarc.fr. 2013

[26] Filella, Xavier ; Foj, Laura ; Augé, Josep M. ; Molina, Rafael ; Alcover, Joan: Clinical utility of p2PSA and prostate health index in the detection of prostate cancer. In: *Clinical Chemistry And Laboratory Medicine: CCLM / FESCC* 52 (2014), Nr. 9, p. 1347 – 1355. – ISSN 1434–6621

[27] G. Litjens, W. Ven N. K. ; Huisman, H.: A pattern recognition approach to zonal segmentation of the prostate on mri. In: *Proceedings of the 15th international conference on Medical Image Computing and Computer-Assisted Intervention Miccai 2*, 2012, p. 413–420

[28] Gao, Y. ; Tannenbaum, A.: Combining atlas and active contour for automatic 3d medical image segmentation. In: *Biomedical Imaging: From Nano to Macro, IEEE International Symposium on*, 2011, p. 1401–1404

[29] Geert Litjens, Nico K. ; Huisman, Henkjan: A multi-atlas approach for prostate segmentation in MR images. In: *Promise Miccai 2012 Grand Challenge on Prostate MR Image Segmentation*, 2012

[30] Bram van Ginneken, Geert Litjens Rob T. *Miccai: 2012 prostate segmentation challenge MICCAI*

[31] Guan, Huaiqun ; Dong, Hang: Dose calculation accuracy using cone-beam CT (CBCT) for pelvic adaptive radiotherapy. In: *Physics in Medicine and Biology* 54 (2009), Nr. 20, p. 6239

[32] H. Bay, T. T. ; Gool, L. V.: Speeded-up robust features (surf). In: *Comput. Vis. Image Underst.* 110 (2008), p. 346–359

[33] H. Huang, F. M. ; McColl, R.: High dimensional statistical shape model for medical image analysis. In: *Biomedical Imaging: From Nano to Macro, ISBI. 5th IEEE International Symposium on* (2008), p. 1541–1544

[34] H. Pu, M. X. ; Yan, B.: A method in medical image registration based on normalized mutual information. In: *Communication Software and Networks (ICCSN), 2011 IEEE 3rd International Conference on*, 2011, p. 342–346

[35] Heimann, T. ; Meinzer, H.: Statistical shape models for 3d medical image segmentation: A review. In: *Medical Image Analysis* 13(4) (2009), p. 543–563

[36] Hill, A. ; Taylor, C.J.: Model-based image interpretation using genetic algorithms. In: *Image and Vision Computing* 10 (1992), p. 295–300

[37] III, Mack R. ; Faillace-Akazawa, Pamela ; Malfatti, Christine ; Holland, John ; Hricak, Hedvig: Prostate volumes defined by magnetic resonance imaging and computerized tomographic scans for three-dimensional conformal radiotherapy. In: *International Journal of Radiation Oncology*Biology*Physics* 35 (1996), Nr. 5, p. 1011 – 1018. – ISSN 0360–3016

[38] J. Bailleul, S. R. ; Constans, J.M.: Statistical shape model-based segmentation of brain mri images. In: *Engineering in Medicine and Biology Society, EMBS. 29th Annual International Conference of the IEEE* (2007), p. 5255–5258

[39] J. Chappelow, S. Motwani S. Punekar H. Lin S. Both N. Vapiwala S. Hahn A. Madabhushi N. C. ; Toth, R.: Concurrent segmentation of the prostate on mri and ct via linked statistical shape models for radiotherapy planning. In: *Medical physics* (2012), p. 2214–2228

[40] J. Dowling, P. Greer S. O. ; Salvado, O.: Automatic atlas-based segmentation of the prostate. In: *MICCAI 2009 Prostate segmentation challenge*, 2009, p. 1–8

[41] J. Fripp, S. W. ; Ourselin, S.: Automatic Initialization of 3D Deformable Models for Cartilage Segmentation. In: *Digital Image Computing: Techniques and Applications, DICTA. Proceedings*, 2005, p. 74–74

[42] J. Kittler, R. P W D. ; Mata, J.: On combining classifiers. In: *Pattern Analysis and Machine Intelligence, IEEE Transactions* 20 (3) (1998), p. 226–239

[43] J.A. Dowling, S. Chandra J.P.W. Pluim J. Lambert J. Parker J. Denham P.B. G. ; Salvado, O.: Fast automatic multiatlas segmentation of the prostate from 3d

mr images. In: *Proceedings of the 2011 international conference on Prostate cancer imaging: image analysis and image-guided interventions, MICCAI'11* (2011), p. 10–21

[44] J.N. Sarvaiya, S. P. ; Bombaywala, S.: Image Registration by Template Matching Using Normalized Cross-Correlation. In: *Advances in Computing, Control, Telecommunication Technologies, ACT '09. International Conference on*, 2009, p. 819–822

[45] J.P.W. Pluim, J.B.A. M. ; Viergever, M.A.: Mutual-information-based registration of medical images: a survey. In: *Medical Imaging, IEEE Transactions on* 22(8) (2003), p. 986–1004

[46] J.V. Manjón, J.J. Lull G. García-Martí L. Martí-Bonmatí ; Robles, M.: MRI denoising using Non-Local Means. In: *Medical Image Analysis*, 2008, p. 514–523

[47] Kagawa, Kazufumi ; Lee, W.Robert ; Schultheiss, Timothy E. ; Hunt, Margie A. ; Shaer, Andrew H. ; Hanks, Gerald E.: Initial clinical assessment of CT-MRI image fusion software in localization of the prostate for 3D conformal radiation therapy. In: *International Journal of Radiation Oncology*Biology*Physics* 38 (1997), Nr. 2, p. 319 – 325. – ISSN 0360–3016

[48] Krishnan, K. ; Cheung, R.: Evaluation of the accuracy of deformable registration of prostate mri for targeted prostate cancer radiotherapy. In: *Medical Imaging 2009: Image Processing* 7259 (2009), p. 725935–725935–10

[49] L. Florack, M. V. ; Koenderink, J.: The gaussian scale-space paradigm and the multiscale local jet. In: *Int. J. Comput. Vision* 18 (1996), p. 61–75

[50] László, G.N. ; Jayaram, K.U.: On standardizing the MR image intensity scale. In: *Radiology*, 1998, p. 581–582

[51] Liao, S. ; Shen, D.: A feature-based learning framework for accurate prostate localization in ct images. In: *Image Processing, IEEE Transactions on* 21(8) (2012), p. 3546–3559

[52] Liga Colombiana Contra el Cancer. *Cancer de prostata. Deteccion temprana*. Colombia: Liga Colombiana Contra el Cancer. Available: http://www.ligacancercolombia.org/. 2014

[53] Lindeberg, T.: Feature detection with automatic scale selection. In: *Int.J. Comput. Vision* 30 (1998), p. 79–116

[54] M. Erdt, P. S. ; Wesarg, S.: Multi-layer deformable models for medical image segmentation. In: *Information Technology and Applications in Biomedicine (ITAB), 10th IEEE International Conference on*, 2010, p. 1–4

[55] M. Kass, A. W. ; Terzopoulos, D.: Snakes: Active contour models. In: *International Journal of Computer Vision* 1(4) (1988), p. 321–331

[56] M. Kirschner, F. J. ; Wesarg, S.: Automatic prostate segmentation in mr images with a probabilistic active shape model. In: *Promise Miccai 2012 Grand Challenge on Prostate MR Image Segmentation*, 2012, p. 28–35

[57] M. Samiee, G. T. ; Fazel-Rezai, R.: Semi-automatic prostate segmentation of mr images based on flow orientation. In: *Signal Processing and Information Technology, IEEE International Symposium*, 2006, p. 203–207

[58] M. ÃŒzÃ¼mcÃ¼, J.H.C. R. ; Lelieveldt, B.P.F.: Independent component analysis in statistical shape models. In: *SPIE Medical Imaging* (2003), p. 375–383

[59] Maan, B. ; van der Heijden, F.: Prostate mr image segmentation using 3d active appearance models. In: *Promise Miccai 2012 Grand Challenge on Prostate MR Image Segmentation*, 2012, p. 44–51

[60] Makni, Nasr ; Puech, P. ; Lopes, R. ; Dewalle, A.S. ; Colot, O. ; Betrouni, N.: Combining a deformable model and a probabilistic framework for an automatic 3D segmentation of prostate on MRI. In: *International Journal of Computer Assisted Radiology and Surgery* 4 (2009), Nr. 2, p. 181–188. – ISSN 1861–6410

[61] Martin, J. ; Crowley, J.L.: Comparison of Correlation Techniques. In: *Conference on Intelligent Autonomous Systems, IAS '95*, 1995, p. 86–93

[62] Martin, Sébastien ; Daanen, Vincent ; Troccaz, Jocelyne: Atlas-based prostate segmentation using an hybrid registration. In: *International Journal of Computer Assisted Radiology and Surgery* 3(6) (2008), p. 485–492

[63] Martínez, Fabio ; Acosta, Oscar ; de Crevoisier, Renaud ; Romero, Eduardo. *Local jet features and statistical models in a hybrid Bayesian framework for prostate estimation in CBCT images*. 2012

[64] McInerney, T. ; Terzopoulos, D.: Deformable models in medical image analysis: a survey. In: *Medical Image Analysis* 1(2) (1996), p. 91–108

[65] M.D., Liesbeth J. B. ; Ph.D. ; van den Brink M.Sc., Mandy ; M.D., Allison M. B. ; M.D., Tarek S. ; M.Sc., Luuk G. ; te Velde M.Sc., Annet ; M.D., Joos V. L. ; Ph.D.: Estimation of the Incidence of Late Bladder and Rectum Complications After High-Dose (70-78 Gy) Conformal Radiotherapy for Prostate Cancer, Using Dose-Volume Histograms 1. In: *International Journal of Radiation Oncology*Biology*Physics* 41 (1998), Nr. 1, p. 83 – 92. – ISSN 0360–3016

[66] Milborrow, S. ; Nicolls, F.: Locating facial features with an extended active shape model. In: *Proceedings of the 10th European Conference on Computer Vision: Part IV*, 2008, p. 504–513

[67] Milosevic, Michael ; Voruganti, Sachi ; Blend, Ralph ; Alasti, Hamideh ; Warde, Padraig ; McLean, Michael ; Catton, Pamela ; Catton, Charles ; Gospodarowicz, Mary: Magnetic resonance imaging (MRI) for localization of the prostatic apex: comparison to computed tomography (CT) and urethrography. In: *Radiotherapy and Oncology* 47 (1998), Nr. 3, p. 277 – 284. – ISSN 0167–8140

[68] Muja, M. ; Lowe, D.G.: Fast approximate nearest neighbors with automatic algorithm configuration. In: *Visapp* 1 (2009), p. 331–340

[69] N. Makni, R. Lopes A.S. Dewalle O. C. ; Betrouni, N.: Toward automatic zonal segmentation of prostate by combining a deformable model and a probabilistic framework. In: *Biomedical Imaging: From Nano to Macro, ISBI. 5th IEEE International Symposium on*, 2008, p. 69–72

[70] N. Makni, R. Lopes R. Viard O. C. ; Betrouni, N.: Automatic 3d segmentation of prostate in mri combining a priori knowledge, markov fields and bayesian framework. In: *Engineering in Medicine and Biology Society, EMBS 30th Annual International Conference of the IEEE* (2008), p. 2992 –2995

[71] O. Ourselin, S. P. ; Ayache, N.: Block Matching: A General Framework to Improve Robustness of Rigid Registration of Medical Images. In: *Medical Image Computing and Computer-Assisted Intervention - MICCAI 2000*, 2000, p. 557–566

[72] Osher, S. ; Sethian, J.A.: Fronts propagating with curvature-dependent speed: algorithms based on hamilton-jacobi formulations. In: *J. Comput. Phys* 79(1) (1988), p. 12–49

[73] Ou, Y. ; Doshi, J. ; Erusa, G. ; Davatzikos, C.: Multi-atlas segmentation of the prostate: A zooming process with robust registration and atlas selecion. In: *Promise Miccai 2012 Grand Challenge on Prostate MR Image Segmentation*, 2012, p. 60–65

[74] P. Krasnopevtsev, T. P. ; Kryvanos, A.: A statistical approach to automatic heart segmentation and modelling from multiple modalities. In: *Computer-Based Medical Systems, CBMS. 21st IEEE International Symposium on* (2008), p. 44–46

[75] P. Liang, X. Z. ; Jiguang, D.: Fast normalized cross-correlation image matching based on multiscale edge information. In: *Computer Application and System Modeling (ICCASM), 2010 International Conference on* 10 (2010), p. 507–511

[76] Q. Feng, S. Tang W. C. ; Shen, D.: Segmenting ct prostate images using population and patient-specific statistics for radiotherapy. In: *Medical Physics* (2009), p. 282–285

[77] Q. Gao, D. R. ; Edwards, P.E.: An automatic multi-atlas based prostate segmentation using local appearance-specific atlases and patch-based voxel weighting. In: *Promise Miccai 2012 Grand Challenge on Prostate MR Image Segmentation*, 2012, p. 12–19

[78] Quilty, P.M. ; Kirk, D. ; Bolger, J.J. ; Dearnaley, D.P. ; Lewington, V.J. ; Masone, M.D. ; Reed, N.S.E. ; Russell, J.M. ; Yardley, J.: A comparison of the palliative effects of strontium-89 and external beam radiotherapy in metastatic prostate cancer. In: *Radiotherapy and Oncology* 31 (1994), Nr. 1, p. 33 – 40. – ISSN 0167–8140

[79] R. Malladi, J.A. S. ; Vemuri, B.C.: Shape modeling with front propagation: a level set approach. In: *Pattern Analysis and Machine Intelligence, IEEE Transactions on* 17(2) (1995), p. 158–175

[80] R. Toth, M. Rosen G. Reed J. Kurhanewicz A. Kalyanpur-S. P. ; Madabhushi, A.: A magnetic resonance spectroscopy driven initialization scheme for active shape model based prostate segmentation. In: *Medical Image Analysis* 15(2) (2011), p. 214–225

[81] R. Toth, R. S. ; Madabhushi, A.: Medial axis based statistical shape model (massm): Applications to 3d prostate segmentation on mri. In: *Biomedical Imaging: From Nano to Macro, IEEE International Symposium on* (2011), p. 1463–1466

[82] R. Zewail, A. E. ; Durdle, N.: Wavelet-based independent component analysis for statistical shape modeling. In: *Electrical and Computer Engineering, CCECE. Canadian Conference on* (2007), p. 1325–1328

[83] Rasch, Coen ; Barillot, Isabelle ; Remeijer, Peter ; Touw, Adriaan ; van Herk, Marcel ; Lebesque, Joos V.: Definition of the prostate in {CT} and MRI: a multi-observer study. In: *International Journal of Radiation Oncology*Biology*Physics* 43 (1999), Nr. 1, p. 57 – 66. – ISSN 0360–3016

[84] Roweis, S.: Em algorithms for pca and spca. In: *Advances in Neural Information Processing Systems* 10 (1998)

[85] S. Dhamodharan, DR.V. Subbiah B.: Medical image feature, extraction, selection and classification. In: *International Journal of Engineering Science and Technology* 2(6) (2010), p. 2071–2076

[86] S. Ghose, R. Martí X. Lladó J.C. Vilanova J. Freixenet-J. Mitra D. S. ; Meriaudeau, F.: A survey of prostate segmentation methodologies in ultrasound, magnetic resonance and computed tomography images. In: *Comput. Methods Prog. Biomed.* 108(1) (2012), p. 262–287

[87] S. Ghose, R. Martií X. Llado J. Freixenet J.C. V. ; Meriaudeau, F.: Prostate segmentation with texture enhanced active appearance model. In: *Signal-Image Technology and Internet-Based Systems (SITIS), 2010 Sixth International Conference on*, 2010, p. 18–22

[88] S. Klein, I. Lips M. Vulpen M. S. ; Pluim, J.: Automatic segmentation of the prostate in 3d mr images by atlas matching using localized mutual information. In: *Medical Physics* 35 (2008), p. 1407–1417

[89] S.K. Warfield, K.H. Z. ; Wells, W.M.: Simultaneous truth and performance level estimation (STAPLE): an algorithm for the validation of image segmentation. In: *Medical Imaging, IEEE Transactions* 23 (7) (2004), p. 903–921

[90] S.M. Pizer, S. Joshi A. Thall J.Z. Chen Y. Fridman-D.S. Fritsch A.G. Gash J.M. Glotzer M.R. Jiroutek C. Lu K.E. Muller G. Tracton P. Y. ; Chaney, E.L.: Deformable m-reps for 3d medical image segmentation. In: *Int. J. Comput. Vision* 55(2-3) (2003), p. 85–106

[91] S.S. Chandra, K. Shen P. Raniga J.P.W. Pluim P.B. Greer-O. S. ; Fripp, J.: Patient specific prostate segmentation in 3-d magnetic resonance images. In: *Medical Imaging, IEEE Transactions on* 31(10) (2012), p. 1955–1964

[92] T.F. Cootes, D.H. C. ; Graha, J.: Active shape models-their training and application. In: *Computer Vision and Image Understanding* 61(1) (1995), p. 38–59

[93] T.F. Cootes, G. E. ; Taylor, C.J.: Comparing active shape models with active appearance models. In: *Proc. British Machine Vision Conf*, 1999, p. 173–182

[94] T.F. Cootes, G.J. E. ; Taylor, C.J.: Active appearance models. In: *Computer Vision, ECCV98* 1407 (1998), p. 484–498

[95] Thirion, J.P.: Image matching as a diffusion process: an analogy with maxwell's demons. In: *Medical Image Analysis* 2(3) (1998), p. 243–260

[96] Thompson, Ian M. ; Tangen, Catherine M. ; Paradelo, Jorge ; Lucia, M. S. ; Miller, Gary ; Troyer, Dean ; Messing, Edward ; Forman, Jeffrey ; Chin, Joseph ; Swanson, Gregory ; Canby-Hagino, Edith ; Crawford, E. D.: Adjuvant Radiotherapy for Pathological {T3N0M0} Prostate Cancer Significantly Reduces Risk of Metastases and Improves Survival: Long-Term Followup of a Randomized Clinical Trial. In: *The Journal of Urology* 181 (2009), Nr. 3, p. 956 – 962. – ISSN 0022–5347

[97] Toth, R. ; Madabhushi, A.: Deformable landmark-free active appearance models: Application to segmentation of multi-institutional prostate mri data. In: *Promise Miccai 2012 Grand Challenge on Prostate MR Image Segmentation* (2012), p. 67–74

[98] Tsechpenakism, G.: Deformable model-based medical image segmentation. In: *Multi Modality State-of-the-Art Medical Image Segmentation and Registration Methodologies, Springer US*, 2011, p. 33–67

[99] X. Gual-Arnau, F. L. ; Roldan, S.: Organ contouring for prostate cancer: inter-observer and internal organ motion variability. In: *Comput Med. Imaging Graph* 29(8) (2005), p. 639–647

[100] X. Liu, M.A. Haider-T.H. van d. W. ; Yetik, I.S.: Unsupervised segmentation of the prostate using mr images based on level set with a shape prior. In: *Engineering in Medicine and Biology Society, EMBC. Annual International Conference of the IEEE*, 2009, p. 3613–3616

[101] Y. Artan, M.A. H. ; Yetik, I.S.: Graph-based active contours using shape priors for prostate segmentation with mri. In: *Biomedical Imaging: From Nano to Macro, IEEE International Symposium on*, 2011, p. 1459–1462

[102] Y. Gao, S. L. ; Shen, D.: Prostate segmentation by sparse representation based classification. In: *Med Phys* 39 (10) (2012), p. 6372–6387

[103] Y. Xiang, A.C.S. C. ; Ye, J.: An active contour model for image segmentation based on elastic interaction. In: *Journal of Computational Physics* 219(1) (2006), p. 455–476

[104] Yan, P. ; Kassim, A.A.: Medical image segmentation using minimal path deformable models with implicit shape priors. In: *Information Technology in Biomedicine, IEEE Transactions on* 10(4) (2006), p. 677–684

[105] Zelefsky, Michael J. ; Fuks, Zvi ; Happersett, Laura ; Lee, Henry J. ; Ling, C.Clifton ; Burman, Chandra M. ; Hunt, Margie ; Wolfe, Theresa ; Venkatraman, E.S ; Jackson, Andrew ; Skwarchuk, Mark ; Leibel, Steven A.: Clinical experience with intensity modulated radiation therapy (IMRT) in prostate cancer. In: *Radiotherapy and Oncology* 55 (2000), Nr. 3, p. 241 – 249. – ISSN 0167–8140